ACS OMEGA

http://pubs.acs.org/journal/acsodf

Article

Multi-technique Approach to Unravel the (Dis)order in Amorphous Materials

Francesco Tavanti* and Arrigo Calzolari

Cite This: *ACS Omega* 2022, 7, 23255−23264

Read Online

ACCESS | Metrics & More | Article Recommendations | Supporting Information

ABSTRACT: The concept of order in disordered materials is the key to controlling the mechanical, electrical, and chemical properties of amorphous compounds widely exploited in industrial applications and daily life. Rather, it is far from being understood. Here, we propose a multi-technique numerical approach to study the order/disorder of amorphous materials on both the short- and the medium-range scale. We combine the analysis of the disorder level based on chemical and physical features with their geometrical and topological properties, defining a previously unexplored interplay between the different techniques and the different order scales. We applied this scheme to amorphous GeSe and GeSeTe chalcogenides, showing a modulation of the internal disorder as a function of the stoichiometry and composition: Se-rich systems are less ordered than Ge-rich systems at the short- and medium-range length scales. The present approach can be easily applied to more complex systems containing three or more atom types without any a priori knowledge about the system chemical−physical features, giving a deep insight into the understanding of complex systems.

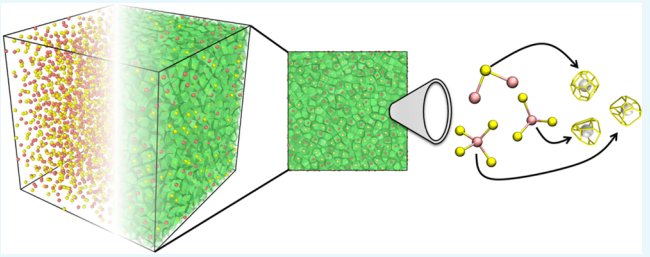

1. INTRODUCTION

Non-crystalline materials, such as amorphous metals, alloys, and glasses, are employed in a wide range of industrial processes and applications.[1,2] The atomic arrangement of disordered systems determines their physical, mechanical, chemical, and electrical properties.[3−6] Several studies showed a strong correlation between the configurational local order and the electronic,[7,8] magnetic, catalytic, and corrosion-resistance properties of disordered systems, as found, for example, for the high-entropy alloys.[9,10] The structural order in amorphous solids is difficult to characterize, and it is far from being understood.[11] Despite the lack of translational periodicity, amorphous systems are not completely random, being organized in hierarchical local structures at different length scales.[12−14] The presence of microscopic-ordered arrangement, repetitive units, or defects is responsible for the macroscopic properties of the whole material. Thus, the description and the evaluation of the order/disorder levels are crucial for the characterization of non-crystalline materials.

Sub-nanometer structures define the so-called short-range order (SRO) of materials and are routinely classified in terms of the chemical coordination properties (e.g., bond type and bond length), as described by the radial distribution function, $g(r)$, analysis.[10] Although very intuitive, this tool does not provide a conclusive understanding of the spatial arrangement of amorphous materials because it averages over a three-dimensional (3D) distribution. Other methods, such as angle distribution functions (ADFs), are used to find the geometry and to extend the length scale of the SRO to the first neighbor shell. Both $g(r)$ and ADFs have been largely used in the field of amorphous semiconductors (e.g., a-Si and SiO_2), where the strong covalent bond fairly resembles the local order arrangement of the crystalline systems.[15,16] However, for systems that do not have a crystalline counterpart (e.g., off-stoichiometric compounds) or the number of components is higher than two (e.g., doped systems and multielement alloys), the analysis techniques based on chemical/physics intuitions become quickly unfeasible due to the rapid increase in the variables (bonding types, interatomic distances, angles, etc.) and in the possible configurations.

The same techniques completely fail in the description of the medium-range order (MRO), which describes how short-range structures combine and connect on the nanometer scale (1−10 nm). In order to overcome this issue, alternative geometrical approaches (such as Voronoi tessellation[17,18] and homology analysis[11,19]) have been developed to investigate the MRO in generic disordered systems, including multielement alloys and metallic glasses.[20] Unfortunately, these approaches, having a purely geometrical foundation, are not able either to

Received: March 7, 2022
Accepted: May 10, 2022
Published: June 24, 2022

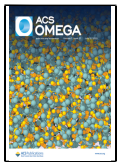

correlate the results with the material composition or to connect with SRO structures.

For these reasons, accurate and versatile tools that are able to describe the hierarchical connections between the SRO and MRO are highly desirable. Here, we employed extended computer simulations and complementary multiscale analysis tools to study the SRO and MRO of amorphous materials. The innovation of the multi-technique study proposed here relies not only on the deep understanding of disordered systems but also on the connections between different analysis approaches which describe the order at different length scales. Starting from the $g(r)$ and the bond angle distributions (BADs) for the detection of the SRO, we move to the MRO by using Voronoi tessellation and homology analysis, finding connections between different analysis methodologies. This allows us to recover the physical insights from the purely structural characterization of the system.

This scheme has been applied to the case of amorphous Ge_xSe_{1-x} chalcogenides with different compositions ($0.4 \leq x \leq 0.6$). Ge_xSe_{1-x} compounds have been proposed for a wide range of applications, including non-volatile memories, photovoltaics, and nanophotonics devices.[21−23] In particular, recent results indicate that Ge_xSe_{1-x} exhibit ovonic electrical switching and that even moderate modulation of the stoichiometry ratio affects the electrical response of the device, whose origin has been ascribed to structural disorder.[21,24] Ge_xSe_{1-x} are characterized by the co-existence of SRO and MRO structures, which vary as a function of the chemical stoichiometry.[10] This allows us to investigate the effect of the composition on the structural order of the system, without changing the number of the chemical species. Even though relatively simple from the chemical point of view (i.e., two species), the choice of Ge_xSe_{1-x} gives also the opportunity to investigate the effects of hetero-atom binding and partially covalent interactions on the SRO and MRO arrangements. The capabilities of the integrated protocol are finally explored in the case of the ternary alloy $(Ge_{0.5}Se_{0.5})_{0.85}Te_{0.15}$.

Our combined approach is able (i) to distinguish between different stoichiometries, (ii) to give a comparison of the relative internal order of chalcogenides systems, and (iii) to be easily extended to systems with three or more elements, for which the number of internal configurations quickly diverges, and the question about the order/disorder level is totally unsolved. This realizes a step forward in the microscopic understanding of the interplay between stoichiometries/compositions and the structural (dis)order of amorphous systems, paving the way to a characterization of the overall mechanical and electrical properties[4,5,7] at the macroscopic level.

2. THEORY AND METHODS

2.1. Order Analysis. In this section, we introduce and briefly review the main statistical tools that we adopted in this work, focusing on their advantages and limitations in describing disordered systems. More details on single analysis techniques can be found in the Supporting Information (SI) file.

2.1.1. Radial Distribution Function. The most common analysis tool to study the atomic packing in the SRO is the RDF or $g(r)$. The $g(r)$ is based on the evaluation of the average atomic density around a central atom and is computed as[25]

$$g(r) = \frac{1}{4\pi r^2 N \rho_0} \sum_{i,j}^{N} \langle \delta(r - |r_i - r_j|) \rangle \quad (1)$$

where r_i is the position of the i-th atom, N the total number of atoms, and ρ_0 is the atomic number density. The RDF gives the distribution of distances from a central atom where peaks represent the most probable distances of remaining atoms with respect to the central one (see Figure S1 in the Supporting Information). The RDF is used to characterize the local structures on the short range obtaining the interatomic distances in that specific system, and it is able to discriminate between different phases of the systems (e.g., liquid vs glass state).[10] However, $g(r)$ is a radial property resulting from the 3D spatial average, and part of the information is lost, such as the angles of the first shell of neighbors and the atomic arrangement for atoms far away from the central one. The RDF in this work has been computed using the VMD plugin.[26]

2.1.2. Bond Local Order. The spatial connectivity of the system is obtained by using in-house bond element lattice local order (BELLO) software.[27] This tool returns the number of atoms connected to a central atom, that is, its FOLD, and how an atom lying within a cutoff radius is spatially arranged in terms of BAD. This analysis describes how atoms arrange to form ordered structures (such as dimers, trimers, and tetrahedral octahedral) based on the orientational parameter q, which is defined as[10,28]

$$q = 1 - \frac{3}{8} \sum_{j,k=1}^{N} \left(\cos\psi_{jk} + \frac{1}{3} \right)^2 \quad (2)$$

where ψ_{jk} is the angle formed by a central atom with its N neighbors, and it has been computed inside the BELLO code.[27] The q-value spans the range from −3 to 1, but it depends on the number of folds, see Figure S2 (Supporting Information). For example, in the case of four-FOLD atoms (four atoms connected to a central one), q runs from 0 that represents a disordered system (e.g., ideal gas) to 1 that represents a perfectly ordered tetrahedral network (e.g., Si bulk).

Using the BAD, we can decompose the results for each FOLD, obtaining information on how different folded atoms spatially arrange and how they are distributed around a central atom. This technique analyzes all possible conformations across the simulation box, but it is limited to the first neighbor shell of each atom, and it becomes computationally demanding for systems with several elements because the number of angles of each species increases exponentially making its application practically unfeasible for systems with three or more elements.

2.1.3. Voronoi Tessellation. In order to describe the MRO, we adopted the Voronoi tessellation method,[18] which has been initially employed in the field of metallic glasses.[29−31] At odds with the approaches discussed above that are driven by bond orientation, the Voronoi approach relies on purely geometrical assessments, being the decomposition of the metric space with respect to a discrete sample of volumetric elements. Thus, a priori chemical or physical characterization of the sample is not required. Each atom is associated with a Voronoi polyhedron (VP), which corresponds to the maximum volume occupied without touching the volume occupied by the neighboring atoms, as illustrated in Figure S3 (Supporting Information). Each VP has a different shape that is identified by the number of faces, n, with m edges (n_m). The VP method does not take

https://doi.org/10.1021/acsomega.2c01359
ACS Omega 2022, 7, 23255−23264

into account the type of the atom, but it only is implicitly connected to the composition of the systems because each atomic environment is intrinsically dependent on the underlying chemistry. By taking into account only the faces with n from three to six (n_3, n_4, n_5, and n_6) and removing the faces that occupy less than the 2% of the total polyhedral surface,[12] we obtained the probability of finding each VP inside the box (see Figure S3, Supporting Information). In this study, the VPs have been computed using Voro++ software.

2.1.4. Multiplicity Indexes. The Voronoi tessellation is used to discriminate among ordered and disordered structures, through the determination of the local-structure multiplicity. Indeed, from the structural point of view, the most important difference between amorphous and crystals is the number of different structures: In crystals, there is one structure which is replicated along the lattice, while amorphous solids have a huge variety of local structures. To quantify the multiplicity of the structures in the sample, we evaluate the so-called Shannon entropy S_h defined as[33]

$$S_h = -\sum_i^n p_i \ln p_i \tag{3}$$

where p_i is the probability to find a specific VP with (n_3, n_4, n_5, and n_6) in the simulation box and n is the number of different VPs. High S_h values (high entropy) reflect a highly disordered system, while values close to 0 (low entropy) represent ordered systems.

Starting from the Shannon index, it is easy to derive the diversity index D that represents the number of distinct structures present inside the simulation box[31]

$$D = \exp(S_h) \tag{4}$$

S_h and D are commonly used for studies on animal and plant populations, but they can be applied also to solid-state problems. For a body-centered cubic structure of a binary system where the two atomic species alternatingly occupy the sites, the value of S_h is 0 and D is 1, meaning that there is a single local structure replicated all over the lattice. In this view, D is able to quantify the multiplicity of structures rather than the frequencies of a few individual structures. These two indexes are not explicitly based on the underlying chemistry of the system but only on its topology. The VP analysis underneath the S_h and D indexes can be read as the indirect connection between the SRO, given by bond lengths and angles of the first neighboring shell, and its MRO, given by the multiplicity of each VP across the box.

Other structural analysis tools, such as the Steinhardt bond-orientational parameters or the X-ray diffraction (XRD) analysis, are also used to investigate the local order and the (lack of) crystallinity in disordered materials. Their definitions and the main properties are reported in the Supporting Information.

2.1.5. Homology Analysis. Persistent homology is an algebraic method to measure the topological features of the shapes that persist at different scales. Its potential has been explored in a wide range of applications, from image analysis to material science.[11,34,35] In this method, each atom is described by a sphere centered in the spatial coordinates (x, y, and z) and a radius parameter, ε, which depends on the atom type. By gradually increasing ε, the spheres can touch each other forming a connected hypersurface. When a closed loop is formed at a given value of ε, we have the event called birth, Birth(ε). Upon increasing again ε, another loop can be formed connecting atoms of the previous loop. In this case, we have the death of the original loop, Death(ε), and the birth of the new one, as shown in Figure S4 (Supporting Information). The radius is increased until no more loops could be found. By plotting the births versus the deaths at a given radius, one can obtain a homology diagram (or persistence diagram, PD); for further details, see the Supporting Information. The PD is a compact descriptor for complex geometrical data sets because it is a translational and rotational invariant, multiscale and robust to noise.[36] The PD approach is able to discriminate among different phases (such as crystalline, liquid, or amorphous) or different stoichiometries of the same compound, having topological distributions that are univocally dependent on the system.

The analysis and the PDs have been computed using the homcloud package of Python,[37] and the measure of the area of the PD distribution has been obtained using the ImageJ package.[38]

Along the lines of the Shannon entropy, it is possible to define an entropy factor (namely, the Persistent entropy, PE) starting from the PD analysis[35]

$$\mathrm{PE} = -\sum_i^n p_i \ln p_i \tag{5}$$

where the probability is given by

$$p_i = \frac{death_i - Birth_i}{\sum_i (Death_i - Birth_i)} \tag{6}$$

PE describes the "topological regularity" that assumes a high value if the structure has a "lattice-like" or regular configuration, while a low PE corresponds to a disordered structure with no consistent patterns.[39]

2.2. System Preparation. The Ge_xSe_{1-x} systems have been simulated by using a classical molecular dynamics (MD) approach, according to Tavanti.[10] Three different stoichiometries have been simulated as follows: $Ge_{0.4}Se_{0.6}$, $Ge_{0.5}Se_{0.5}$, and $Ge_{0.6}Se_{0.4}$. Each system contains 4480 atoms, and the force field (FF) used is based on the well-established Vashishta potential employed for the description at the atomistic level of $GeSe_2$ or InP systems. The classical MD simulations have been carried out by using the LAMMPS package.[43]

Each model system has been melted for 10 ns at 1500 K and then slowly cooled down to 300 K with a cooling rate of 5 K/ps, which ensures a good balance between a low computational cost and a good description of the amorphous structure.[44] Finally, a production run of 50 ns at 300 K has been carried out in an *NVT* ensemble where the temperature is controlled by using the Nosé−Hoover thermostat with a coupling time of 1 ofs, and the timestep used is of 1 fs.

We further considered a three-element alloy $(Ge_{0.5}Se_{0.5})_{0.85}Te_{0.15}$, which maintains the relative concentration of Ge and Se and can be compared with the undoped $(Ge_{0.5}Se_{0.5})$ case. The FF employed is the Vashishta FF as for the GeSe systems where the new charges have been computed by using Rappe and Goddard's QEq scheme using the GULP package,[45] ensuring the charge neutrality of the system. For Te, $\alpha_{Te} = 9$, $\sigma_{Te} = 2.21$, and $\eta_{Te-Te} = 7$, $\eta_{Te-Se} = 7$, and $\eta_{Te-Ge} = 9$. The same simulation protocol of GeSe systems has been employed to produce the liquid and the amorphous phase of the $(Ge_{0.5}Se_{0.5})_{0.85}Te_{0.15}$ system.

https://doi.org/10.1021/acsomega.2c01359
ACS Omega 2022, 7, 23255−23264

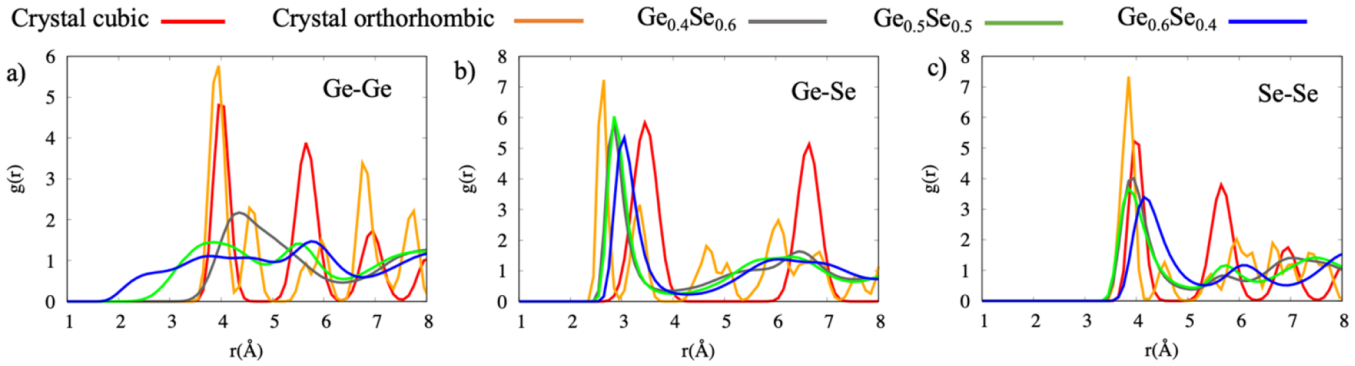

Figure 1. Partial RDFs, $g(r)$, for (a) Ge−Ge, (b) Ge−Se, and (c) Se−Se. Red lines represent the cubic crystal and orange lines the orthorhombic crystals, included for comparison. Gray, green, and blue lines correspond to $Ge_{0.4}Se_{0.6}$, $Ge_{0.5}Se_{0.5}$, and $Ge_{0.6}Se_{0.4}$, respectively.

3. RESULTS AND DISCUSSION

3.1. Chemical−Physical Analysis. Figure 1 displays the partial $g(r)$ distributions for the three Ge_xSe_{1-x} systems resulting from MD simulations. The RDF spectra of the corresponding cubic and orthorhombic crystalline phases have been included for comparison. Peaks belonging to the crystal phases are very sharp with respect to the amorphous phases for homopolar distances (Ge−Ge and Se−Se), while the peaks of the heteropolar distances (Ge−Se) are very similar in both crystal and amorphous systems. The other main difference in the plots is the presence of secondary peaks that are less pronounced in the amorphous cases.

To describe the local atomic aggregation, we study the atomic folding or FOLD, that is, the number of bonds of each atom and the respective angles within a certain cutoff. The results are reported in Figure 2. The first remarkable feature is the lack of a tetrahedral structure ($q \sim 1$) that is the typical feature of semiconductor systems such as Si and SiO_2. On the contrary, 4-FOLD structures ($q \sim 0.85$), which differ from the tetrahedral ones for the angle distribution, are largely present for the $Ge_{0.4}Se_{0.6}$ and $Ge_{0.6}Se_{0.4}$ compositions. This suggests that the abundance of Ge favors four-coordinated aggregates, whose angle distributions move away from the cubic-like symmetry. The 3-FOLD arrangement is common to all systems, while $Ge_{0.4}Se_{0.6}$ is dominated by the 2-FOLD atoms. This implies that the Se-rich compound is weakly networked with respect to the other two, which are mutually similar in terms of FOLDS.

The results, summarized in Figure S5, report on the BAD of Ge_xSe_{1-x} systems, considering all angles among atoms within a 3.0 Å shell. BADs show marked peaks around 90° for the Se−Ge−Se angle of the three systems, while the peak intensity of the Ge−Se−Ge angle decreases at a higher Ge content. The main peak of BADs is progressively shifted from 97 to 78, and a secondary peak at 140° appears on increasing the Ge content. A similar BAD has been found for other Se-rich chalcogenides in the literature.[40−42] This suggests that the increase in the Ge content can generally improve the SRO in amorphous chalcogenides. By decomposing the BAD on the most abundant folds (i.e., 2-FOLD, 3-FOLD, and 4-FOLD atoms), we observe that major contributions come from heteropolar Se−Ge−Se and Ge−Se−Ge angles (Figure S6). This analysis shows that the atomic distribution radically changes with the stoichiometry that affects the network connectivity and the local order, as reported in the Supporting Information. From the combination of the $g(r)$ and BAD analysis, we can conclude that $Ge_{0.5}Se_{0.5}$ is the most ordered

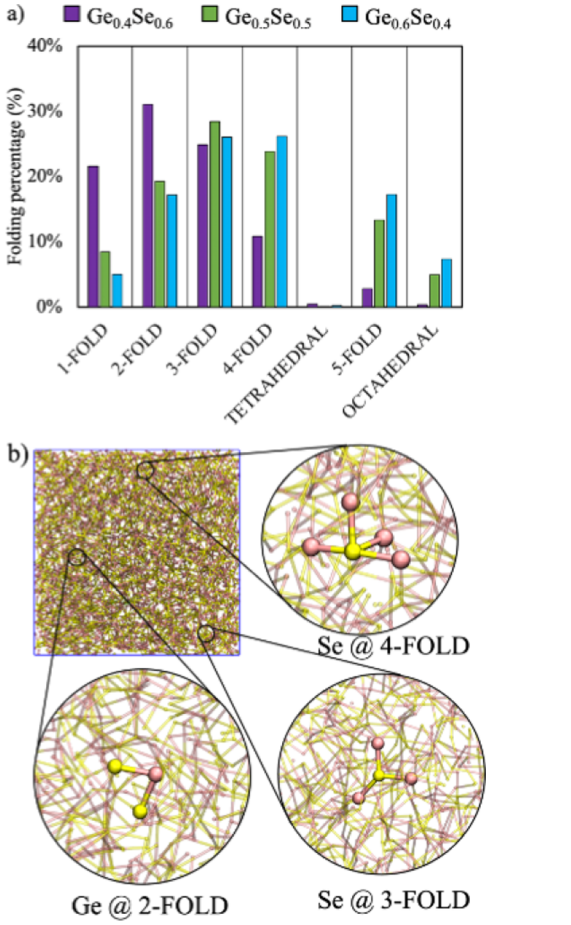

Figure 2. (a) Folding percentage distribution of Ge_xSe_{1-x} systems. The color code corresponds to the legend mentioned above. (b) Atomistic representations of selected FOLDs inside the simulation box.

structure on the short range because it has the highest number of heteropolar bonds closely arranged at 90°, while the $Ge_{0.4}Se_{0.6}$ could be the least ordered one, having a very broad angle distribution.

This discussion clearly shows how the analysis of bond length and angle distribution, albeit conceptually very simple, may become absolutely non-trivial for realistic systems with more than two chemical species (e.g., alloys, doped compounds, etc.). This is evident in the case of the GeSeTe compound, where the change from the binary to ternary

https://doi.org/10.1021/acsomega.2c01359
ACS Omega 2022, 7, 23255−23264

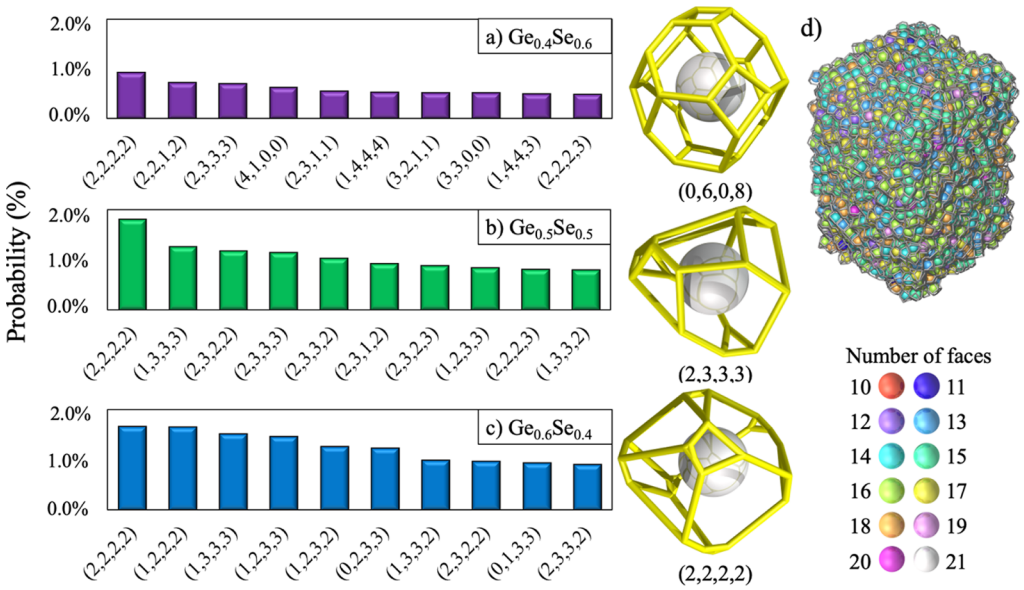

Figure 3. Probability distribution of the 20 most common VPs for Ge_xSe_{1-x} systems, a function of the Ge content: (a) $x = 0.4$, (b) $x = 0.5$, and (c) $x = 0.6$. On the right, the geometrical representation of selected VP structures is shown: (0, 6, 0, 8) is the bcc-like crystal arrangement; (2, 3, 3, 3) and (2, 2, 2, 2) represent two common VPs found in MD simulations. Faces with small probability are not considered in the counting. (d) 3D visualization of the $Ge_{0.5}Se_{0.5}$ system with atoms colored according to the sum of all the faces of each VP.

system increases by a factor of 3 (from 6 to 18) the number of possible configurations, making this kind of analysis practically unfeasible. The results are summarized in Figure S7 in the Supporting Information. We will come back to the interpretation of the order analysis of GeSeTe later in the text.

3.2. Physical versus Geometrical Analysis. We employed the Voronoi tessellation technique[18,32] to have a description of the MRO. The analysis of the most common VPs shows that for Ge_xSe_{1-x} systems, there are several different structures with very low probability, not exceeding the ∼2% in frequency. The most common structures in the simulation box have a probability in the order of 1.8%, but this value is halved very fast as shown in Figure 3. The (2, 2, 2, 2) is one of the most recurrent shapes for all the stoichiometries. Other VP shapes are system-specific: for instance, the (4, 1, 0, 0) has a probability of 0.63% for the $Ge_{0.4}Se_{0.6}$ while only 0.11 and 0.02% for $Ge_{0.5}Se_{0.5}$ and $Ge_{0.4}Se_{0.6}$, respectively. A similar variability has been already detected in metallic glasses.[12,29−31] However, with respect to metallic glasses where common VPs are (0,2,8,2),[31] we detected structures containing abundant n_3 faces but only few n_4, n_5, and n_6 faces. This difference suggests that the Ge_xSe_{1-x} compounds are less faceted than typical metallic glasses.

As can be observed from Figure 3, the VP analysis alone does not provide a conclusive or intuitive description of the structural order at different scales. The multiplicity indexes may help in discriminating among ordered and disordered structures. Notably, both S_h and D indexes are dependent on the size of the simulation cell.[31] In our case, we applied this analysis to two systems: the first is the original one with 4480 atoms per cell, as obtained by MD;[10] the second results from the average over 10 snapshots of the box to increase the sampling to 44,800 points. The results in Table 1 indicate that even though there are a few numerical differences between the values for the single and the enlarged cells, the same trends hold for all the considered stoichiometries. It comes out that $Ge_{0.4}Se_{0.6}$ has more structural variability than the other two systems, which are similar to each other. This trend is confirmed also by the calculation of the Steinhardt parameters reported in the Supporting Information.

Table 1. Shannon and Diversity Indexes for the Three Stoichiometries as a Function of the Number of Atoms per Cell[a]

	number of atoms	$Ge_{0.4}Se_{0.6}$	$Ge_{0.5}Se_{0.5}$	$Ge_{0.6}Se_{0.4}$
Shannon entropy, S_h	4480	6.41	6.11	5.7
	44,800	6.63	6.23	6.08
diversity index, D	4480	608	453	302
	44,800	758	508	441

[a]The values of the S_h and D indexes for 4480 atoms correspond to the single configurations, while the 44,800 atoms refer to the enlarged cell, the resulting average over 10 trajectory snapshots.

3.3. Topological Analysis. The MRO is complex to determine because it implicitly relies on the assembly of SRO structures on a larger spatial scale. To have an accurate view of the MRO, we applied the homology analysis.[19] First, we fix on the 50−50% concentration, and we compare the $Ge_{0.5}Se_{0.5}$ systems in different phases, namely, the cubic crystal, the orthorhombic crystal, the liquid, and the amorphous. The crystal phases are characterized by well-defined distributions due to the fixed distance between atoms. This is responsible for well-marked regions in the PD, as reported in Figure 4a,b. In the case of the liquid phase, atoms are more mobile, and the PD distribution is very broad, with a tail at small values of Death and Birth. In the amorphous phase, the PD distribution is broader than in the crystal phase but sharper than in the liquid phase, and it lacks the characteristic tail at small values (Figure 4c,d). It follows that the broader the distribution, the less ordered the system. This trend is confirmed by the calculation of the surface area covered by the PD, reported in Figure 4. The amorphous phase spans a slightly wider PD area (1.93 Å^2) than the crystal phases (1.74 and 1.70 Å^2) but much lower than the liquid phase (2.35 Å^2).

https://doi.org/10.1021/acsomega.2c01359
ACS Omega 2022, 7, 23255−23264

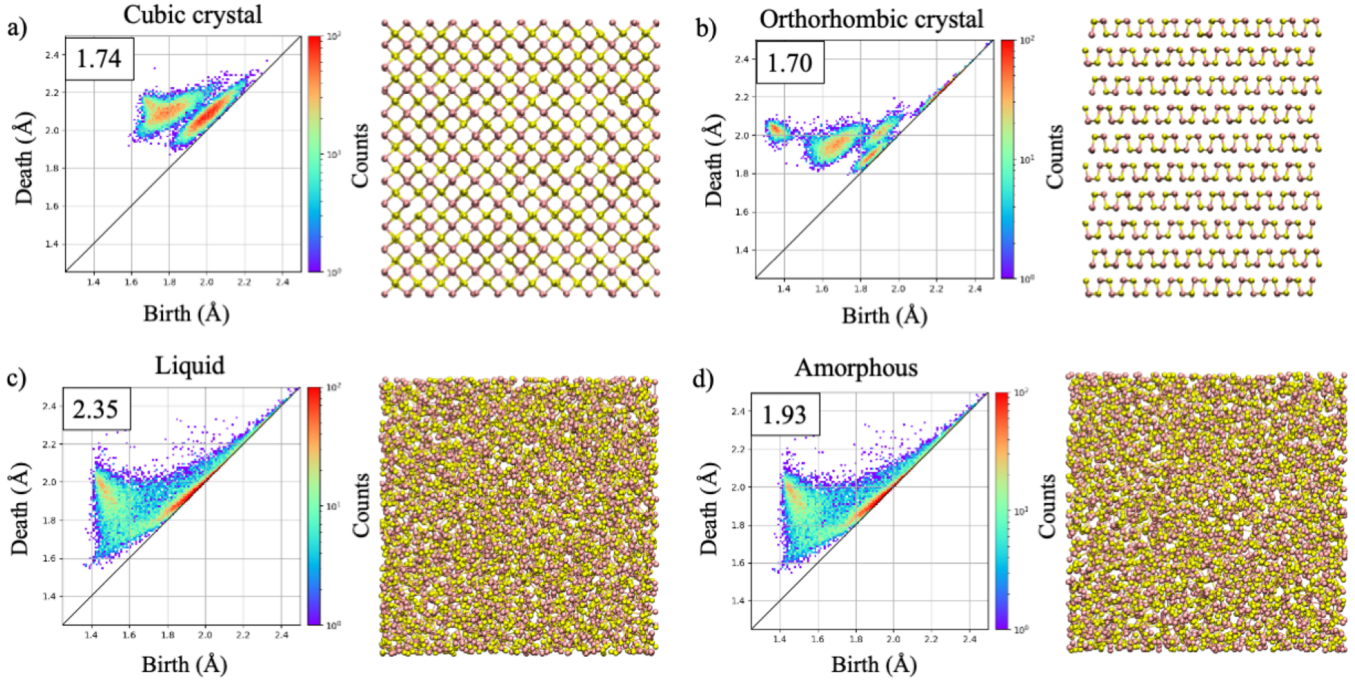

Figure 4. PDs for different phases of $Ge_{0.5}Se_{0.5}$: (a) cubic crystal, (b) orthorhombic crystal, (c) liquid, and (d) amorphous phase. Numbers on the top-left panels represent the area of the PD surface expressed in $Å^3$.

The comparison among the three Ge_xSe_{1-x} stoichiometries is reported in Figure S9. We observed that upon increasing the Ge content, the point distribution shifts from the region close to the diagonal toward the vertical region close to Birth = 2 Å, having points closer to the origin. The PDs for $Ge_{0.5}Se_{0.5}$ and $Ge_{0.6}Se_{0.4}$ are similar, even if the $Ge_{0.5}Se_{0.5}$ distribution looks visually little more compact, suggesting a more ordered structure with respect to $Ge_{0.6}Se_{0.4}$.

This confirms that the PD analysis is able to discriminate between different stoichiometries and aggregation phases. The different surface values allow us also to rank the order level for the systems not only for the amorphous but also for the liquid phase: $Ge_{0.5}Se_{0.5}$ > $Ge_{0.6}Se_{0.4}$ > $Ge_{0.4}Se_{0.6}$. Since lower PE values represent a more disordered structure, we conclude that the Se-rich system is most disordered among the Ge_xSe_{1-x} compounds considered in this work. Notably, the increasing trend of PE anticorrelates with the decreasing trend of the S_h and D indexes, for the same systems (Figure 5). This establishes a first important correlation among the analysis approaches (see below).

To confirm that homology analysis is able to distinguish between different phases of the same system, we generate for each stoichiometry a "fake" amorphous model generated upon an unphysically fast cooling rate (20 K/ps), which results in the formation of a frozen-liquid state. Visually, the PD distributions are similar to those of the amorphous structures, but the measure of their surface increases toward the liquid limit. For example, in the case of $Ge_{0.5}Se_{0.5}$, the area of the PD surface of the "fast quench" structure is 2.03 $Å^2$, which is in between the liquid (2.35 $Å^2$) and the amorphous (1.93 $Å^2$) values. This confirms that the cooling rate drives the final configuration of the solid phase, and it should be carefully chosen depending on the desired effect.[44]

In summary, we can conclude that the Ge-rich system is more ordered than the Se-rich one, on both the short and the medium range. This result was is not obvious a priori since the

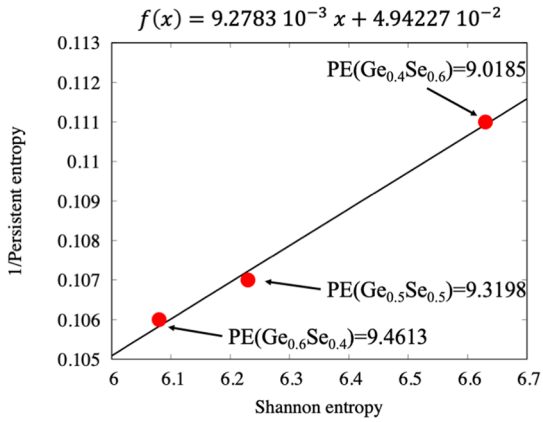

Figure 5. Shannon entropy versus the inverse of the PE (1/PE) for the three amorphous stoichiometries. The red points represent the three systems where labels represent the respective PE value. The black line is the linear fitting curve, and its equation is reported over the graph.

different scale orders have different origins: the SRO in chalcogenides is mainly driven by covalent bonds of first neighbor atoms and is characterized by their bonding distances and angles, while the MRO is disentangled from the chemical connectivity since it relates atoms that are not necessarily covalently bonded.[46]

3.4. Connecting SRO and MRO Analysis. Even though each of the methodologies presented in the previous section generates information useful to describe different aspects of disordered systems, the interconnection among them is not a trivial task since they refer to different theories and describe orders at different scales. This precludes the possibility to draw a coherent characterization of the (dis)order level of the overall material. However, when applied to the same system, these methodologies must be implicitly interconnected throughout the atomic positions. Following this idea, we

https://doi.org/10.1021/acsomega.2c01359
ACS Omega 2022, 7, 23255−23264

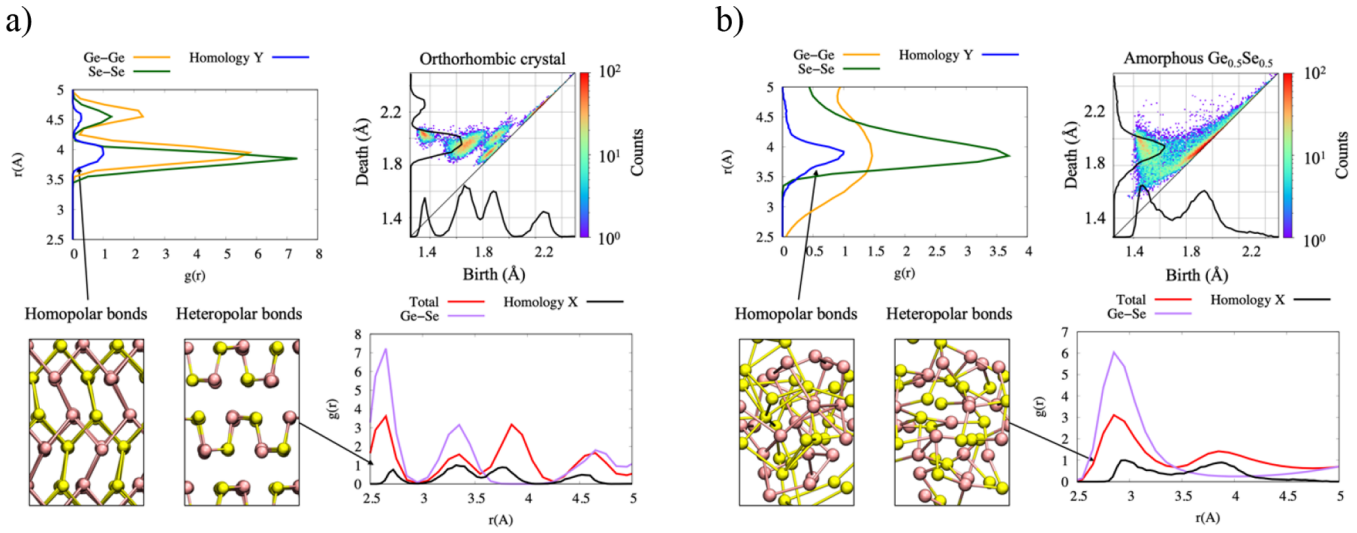

Figure 6. Projection of homology graphs on the Birth axis and comparison with the total and partial $g(r)$ for the orthorhombic crystal (a) and amorphous (b) $Ge_{0.5}Se_{0.5}$.

unravel the interplay between the single pieces of information, connecting the chemical–physical to topological analyses and the short-range to the medium-range structures. We have already underlined the correlation between the Shannon and the PE in the previous section, which relates the Voronoi and the homology realms, through an inverse proportionality relation.

From the homology analysis, it follows that the distribution of distances between atoms forming the closed loops, the Birth events, is comparable to the half of that of the interatomic distances found from the $g(r)$ analysis.[46] Thus, by projecting the points of the homology analysis on the Birth axis, we obtained a distribution similar to the first peak of the $g(r)$, corresponding to the heteropolar Ge–Se bonds, as shown in Figure 6. The first peak from the homology is slightly shifted to higher values with respect to the total $g(r)$ because the first peak of the $g(r)$ is at a distance where the two spheres touch each other for the first time. On the other side, the Birth event atoms are as close as the half of the first peak of the $g(r)$ where the two spheres partially overlap. The projection resembles the $g(r)$ peaks also for the orthorhombic crystal, as reported in Figure 6; the same holds for all other systems studied here (see Figure S10).

By projecting the Death events, we obtained a distribution centered on the second peak of the total $g(r)$, which corresponds to the homopolar Ge–Ge and Se–Se bonds. This suggests that the Birth event is associated to the heteropolar bonds while Death events to homopolar bonds. On the methodological grounds, this opens the possibility to enrich the topological results with the chemical–physical information and thus to have a first coherent connection between the SRO and MRO structure.

The Voronoi analysis can be related to the atomic FOLD, which describes how many atoms are connected to each other based on a cut-off criterion. For instance, one-folded (1-FOLD) atoms describe local structures where only one atom is within the cutoff, while other atoms are at larger distances. In terms of volume, this corresponds to a large free space around the central atom. By contrast, six-folded atoms are connected to other six atoms within a cutoff distance, which corresponds to a small free volume. This can be related to the volume of the VP for each atom. By plotting the volume of the VPs versus the atomic fold of each atom, we observed that low-folded atoms have a higher VP's volume with respect to high-folded atoms where the volume is much smaller, as reported in Figure 7.

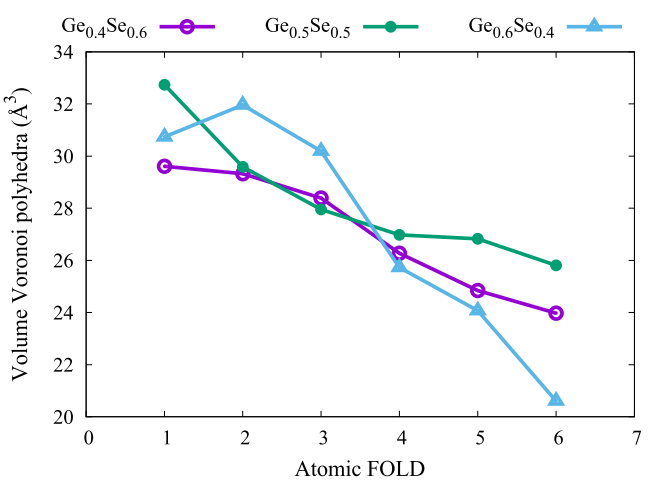

Figure 7. Volume of the VP versus the atomic fold for the three amorphous structures as reported in the legend mentioned above.

Although the single tools were previously known, their interconnected use is the core of the approach proposed here. The integrated methodology allows for a deeper understanding of the order level on the short and medium scales. Figure 8 summarizes the correlation and dependencies among the information derived from the approaches discussed in this work, where blue arrows represent the original outputs and red arrows the linking between them. The common starting point is the atomic structure to which the $g(r)$, Voronoi, and homology analyses are applied. The output of the $g(r)$ is then used as the input to define the cutoff distances for the atomic FOLDs, which are correlated to the free volume obtained from the Voronoi tessellation. The latter analysis gives for each system an estimate of the Shannon entropy which is inversely proportional to the PE coming from the homology analysis. The projection of the Birth and Death events from the homology diagram is back-projected and correlated to the first

https://doi.org/10.1021/acsomega.2c01359
ACS Omega 2022, 7, 23255–23264

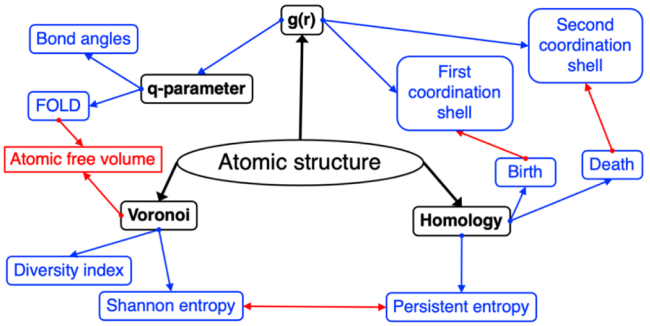

Figure 8. Sketch of the integrated multi-technique approach. The employed techniques are marked in bold, their output in blue, and the connections between them in red. Arrows identify the mutual dependencies.

and second neighbors coming from the $g(r)$, on closing the loop. This makes evident the possibility to link the different scales and recover physical information also from topological results.

3.5. Ternary Systems. As an example of the capability of our integrated approach to go beyond the results of the single components, we considered the case of the ternary alloys $(Ge_{0.5}Se_{0.5})_{0.85}Te_{0.15}$, for which the direct chemical-based analysis is hard to handle. The results are shown in Figure 9. The $g(r)$ for alloys or systems with three elements results in six distributions that are still not complex to understand. By contrast, the application of the local order analysis through the evaluation of FOLD and the BAD statistics is more complex due to the high number of resulting data (see Figure S7 in the Supporting Information). Despite the high accuracy of single pieces of the information on the local atomic arrangement, the extraction of global properties is difficult to grasp. On the contrary, Voronoi tessellation and homology analysis provide an easier characterization of the order at different scales. Thus, the MRO results can be back-traced, to obtain information on the SRO in terms of the chemical−physical parameters. The results are used to interpret the local-order data from, for example, $g(r)$ or FOLD analysis (see red arrows in Figure 8). In the case of $(Ge_{0.5}Se_{0.5})_{0.85}Te_{0.15}$, the presence of 15% of Te imparts a clear change to the diversity index and to the PD, whose area is higher with respect to the $Ge_{0.5}Se_{0.5}$ but much lower than that of the undoped Se-rich system. We can thus conclude that despite the higher number of chemical elements, $(Ge_{0.5}Se_{0.5})_{0.85}Te_{0.15}$ is microscopically more ordered than $Ge_{0.4}Se_{0.6}$.

4. CONCLUSIONS

We outlined a procedure to study the origin of the structural order in amorphous systems that rely on well-known but cutting-edge analysis methodologies. The SRO has been described using the RDF, the atom fold, the BAD, XRD, and the Steinhardt parameters that are all based on chemical and physical assumptions, such as the distance between first neighbors. Then, the MRO has been characterized using the diversity index and the homology analysis, while the connection between the two length scales is obtained using the Voronoi tessellation analysis. Strength and weakness of each employed technique are reported in the Supporting Information. Although these analyses seem independent of each other, they are implicitly related through the atomistic structure, and each of them should be used to understand the

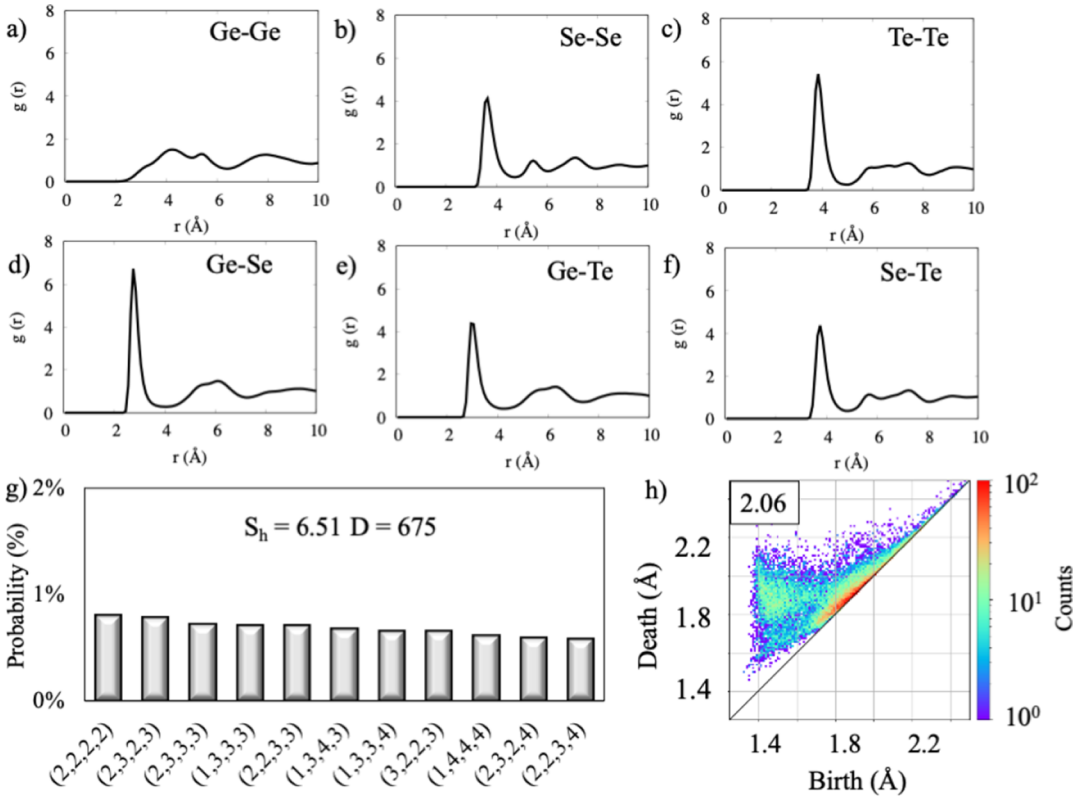

Figure 9. (a−f) RDF of the $(Ge_{0.5}Se_{0.5})_{0.85}Te_{0.15}$ system; (g) probability distribution of the VP with the corresponding S_h and D indexes; and (h) PD with the respective value of the surface area.

https://doi.org/10.1021/acsomega.2c01359
ACS Omega 2022, 7, 23255−23264

origin of the order in amorphous systems. Thus, we demonstrated the correlation among multiple approaches so to connect the chemical and topological properties of the system on both the short and medium range.

The present protocol has been successfully applied to Ge_xSe_{1-x} systems where the relative stoichiometry changes the structural arrangement and order level of the single compounds. We also showed that this pipeline can be easily extended to multi-element compounds [e.g., $(Ge_{0.5}Se_{0.5})_{0.85}Te_{0.15}$] with several bonding interactions (e.g., covalent, polar, dative, etc.) and structural compositions where the classical analysis based on the physical intuitions cannot be applied due to the high number of variables involved.

On a more general ground, the agile approach proposed here allows one to tackle very complex problems, such as the organization of biological systems, for example, proteins, nucleic acids, cells, and so forth, where the different hierarchical structures (e.g., sequence of amino acids, α-helices, and β-sheets in proteins) play the analogous role of the SRO and MRO in the solid-state case..

■ ASSOCIATED CONTENT

Supporting Information

The Supporting Information is available free of charge at https://pubs.acs.org/doi/10.1021/acsomega.2c01359.

Computational details, analysis technique schemes, BADs, Steinhardt and XRD description, and homology analysis comparison and correlation analysis for $Ge_{0.4}Se_{0.6}$ and $Ge_{0.6}Se_{0.4}$ (PDF)

■ AUTHOR INFORMATION

Corresponding Author

Francesco Tavanti − *CNR-NANO Research Center S3, 41125 Modena, Italy;* orcid.org/0000-0002-0594-5308; Email: francesco.tavanti@nano.cnr.it

Author

Arrigo Calzolari − *CNR-NANO Research Center S3, 41125 Modena, Italy;* orcid.org/0000-0002-0244-7717

Complete contact information is available at: https://pubs.acs.org/10.1021/acsomega.2c01359

Author Contributions

F.T. performed the simulations and the analysis. F.T. and A.C. wrote the article. A.C. supervised the work.

Funding

This work was partially funded by EC through H2020-NMBP-TO-IND project GA no. 814487 (INTERSECT) and H2020-NMBP-TO-IND-2018-2020 project GA no. 953167 (Open-Model).

Notes

The authors declare no competing financial interest.

The data sets generated during and analyzed during the current study are available from the corresponding author on reasonable request.

■ ACKNOWLEDGMENTS

We thank Dr. A. Catellani and Dr. B. Dianat for fruitful discussion.

■ REFERENCES

(1) Salinas-Torres, D.; Nozaki, A.; Navlani-García, M.; Kuwahara, Y.; Mori, K.; Yamashita, H. Recent Applications of Amorphous Alloys to Design Skeletal Catalysts. *Bull. Chem. Soc. Jpn.* **2020**, *93*, 438−454.

(2) Jiang, H.; Shang, T.; Xian, H.; Sun, B.; Zhang, Q.; Yu, Q.; Bai, H.; Gu, L.; Wang, W. Structures and Functional Properties of Amorphous Alloys. *Small Struct.* **2021**, *2*, 2000057.

(3) Chai, Z.; Zhang, W.; Degraeve, R.; Clima, S.; Hatem, F.; Zhang, J. F.; Freitas, P.; Marsland, J.; Fantini, A.; Garbin, D.; Goux, L.; Kar, G. S. Dependence of Switching Probability on Operation Conditions in GexSe1-x Ovonic Threshold Switching Selectors. *IEEE Electron Device Letters* **2019**, *40*, 1269.

(4) Telford, M. The Case for Bulk Metallic Glass. *Mater. Today* **2004**, *7*, 36−43.

(5) Song, J.; Zhu, W.; Wei, X. Correlations between the Hierarchical Spatial Heterogeneity and the Mechanical Properties of Metallic Glasses. *Int. J. Mech. Sci.* **2021**, *204*, 106570.

(6) Presti, D.; Muniz-Miranda, F.; Tavanti, F.; Pedone, A. Structure Analysis and Properties Calculations. In *Atomistic Simulations of Glasses*; John Wiley & Sons, Ltd, 2022; pp 89−122.

(7) Yuan, C. C.; Xiang, J. F.; Xi, X. K.; Wang, W. H. NMR Signature of Evolution of Ductile-to-Brittle Transition in Bulk Metallic Glasses. *Phys. Rev. Lett.* **2011**, *107*, 236403.

(8) Yuan, Y.; Kim, D. S.; Zhou, J.; Chang, D. J.; Zhu, F.; Nagaoka, Y.; Yang, Y.; Pham, M.; Osher, S. J.; Chen, O.; Ercius, P.; Schmid, A. K.; Miao, J. Three-Dimensional Atomic Packing in Amorphous Solids with Liquid-like Structure. *Nat. Mater.* **2022**, *21*, 95−102.

(9) Yang, Y.; Zhou, J.; Zhu, F.; Yuan, Y.; Chang, D. J.; Kim, D. S.; Pham, M.; Rana, A.; Tian, X.; Yao, Y.; Osher, S. J.; Schmid, A. K.; Hu, L.; Ercius, P.; Miao, J. Determining the Three-Dimensional Atomic Structure of an Amorphous Solid. *Nature* **2021**, *592*, 60−64.

(10) Tavanti, F.; Dianat, B.; Catellani, A.; Calzolari, A. Hierarchical Short- and Medium-Range Order Structures in Amorphous GexSe1−x for Selectors Applications. *ACS Appl. Electron. Mater.* **2020**, *2*, 2961−2969.

(11) Hiraoka, Y.; Nakamura, T.; Hirata, A.; Escolar, E. G.; Matsue, K.; Nishiura, Y. Hierarchical Structures of Amorphous Solids Characterized by Persistent Homology. *Proc. Natl. Acad. Sci. U.S.A.* **2016**, *113*, 7035.

(12) Sheng, H. W.; Luo, W. K.; Alamgir, F. M.; Bai, J. M.; Ma, E. Atomic Packing and Short-to-Medium-Range Order in Metallic Glasses. *Nature* **2006**, *439*, 419−425.

(13) Zhang, Y.; Zuo, T. T.; Tang, Z.; Gao, M. C.; Dahmen, K. A.; Liaw, P. K.; Lu, Z. P. Microstructures and Properties of High-Entropy Alloys. *Prog. Mater. Sci.* **2014**, *61*, 1−93.

(14) Lee, P. A.; Ramakrishnan, T. V. Disordered Electronic Systems. *Rev. Mod. Phys.* **1985**, *57*, 287−337.

(15) Badro, J.; Teter, D. M.; Downs, R. T.; Gillet, P.; Hemley, R. J.; Barrat, J.-L. Theoretical Study of a Five-Coordinated Silica Polymorph. *Phys. Rev. B: Condens. Matter Mater. Phys.* **1997**, *56*, 5797−5806.

(16) Zhu, W.; Zheng, G.; Cao, S.; He, H. Thermal Conductivity of Amorphous SiO2 Thin Film: A Molecular Dynamics Study. *Sci. Rep.* **2018**, *8*, 10537.

(17) Takada, A. Voronoi Tessellation Analysis of SiO2 Systems Based on Oxygen Packing. *J. Non-Cryst. Solids* **2018**, *499*, 309−327.

(18) Montoro, J. C. G.; Abascal, J. L. F. The Voronoi Polyhedra as Tools for Structure Determination in Simple Disordered Systems. *J. Phys. Chem.* **1993**, *97*, 4211−4215.

(19) Otter, N.; Porter, M. A.; Tillmann, U.; Grindrod, P.; Harrington, H. A. A Roadmap for the Computation of Persistent Homology. *EPJ Data Sci.* **2017**, *6*, 17.

(20) Cheng, Y. Q.; Ma, E. Atomic-Level Structure and Structure−Property Relationship in Metallic Glasses. *Prog. Mater. Sci.* **2011**, *56*, 379−473.

(21) Chai, Z.; Freitas, P.; Marsland, J.; Fantini, A.; Garbin, D.; Goux, L.; Kar, G. S.; Shao, W.; Zhang, W.; Brown, J.; Degraeve, R.; Salim, F. D.; Clima, S.; Hatem, F.; Zhang, J. F. GeSe-Based Ovonic Threshold

Switching Volatile True Random Number Generator. *IEEE Electron Device Lett.* **2020**, *41*, 228−231.
(22) Liu, G.; Li, T.; Wu, L.; Chen, Y.; Liu, B.; Ma, Z.; Song, S.; Song, Z. Increasing Trapped Carrier Density in Nanoscale GeSeAs Films by As Ion Implantation for Selector Devices in 3D-Stacking Memory. *ACS Appl. Nano Mater.* **2019**, *2*, 5373−5380.
(23) Murgatroyd, P. A. E.; Smiles, M. J.; Savory, C. N.; Shalvey, T. P.; Swallow, J. E. N.; Fleck, N.; Robertson, C. M.; Jäckel, F.; Alaria, J.; Major, J. D.; Scanlon, D. O.; Veal, T. D. GeSe: Optical Spectroscopy and Theoretical Study of a van Der Waals Solar Absorber. *Chem. Mater.* **2020**, *32*, 3245−3253.
(24) Ahn, H.-W.; Jeong, D. S.; Cheong, B.-k.; Lee, H.; Lee, H.; Kim, S.-d.; Shin, S.-Y.; Kim, D.; Lee, S. Effect of Density of Localized States on the Ovonic Threshold Switching Characteristics of the Amorphous GeSe Films. *Appl. Phys. Lett.* **2013**, *103*, 042908.
(25) Chandler, D. Introduction to Modern Statistical. *Mechanics*; Oxford University Press: Oxford, U.K., **1987**; Vol. *5*.
(26) Humphrey, W.; Dalke, A.; Schulten, K. VMD: Visual Molecular Dynamics. *J. Mol. Graph.* **1996**, *14*, 27−28.
(27) Dianat, B.; Tavanti, F.; Padovani, A.; Larcher, L.; Calzolari, A. BELLO: A Post-Processing Tool for the Local-Order Analysis of Disordered Systems. *Comput. Mater. Sci.* **2022**, *209*, 111381.
(28) Errington, J. R.; Debenedetti, P. G. Relationship between Structural Order and the Anomalies of Liquid Water. *Nature* **2001**, *409*, 318−321.
(29) Zhang, Q.; Wang, J.; Tang, S.; Wang, Y.; Li, J.; Zhou, W.; Wang, Z. Molecular Dynamics Investigation of the Local Structure in Iron Melts and Its Role in Crystal Nucleation during Rapid Solidification. *Phys. Chem. Chem. Phys.* **2019**, *21*, 4122−4135.
(30) George, S.; Kádas, K.; Jönsson, P. E.; Muscas, G.; Magnus, F.; Eriksson, O.; Delin, A.; Andersson, G. Local Structure in Amorphous SmxCo1-x: A Combined Experimental and Theoretical Study. *J. Mater. Sci.* **2020**, *55*, 12488−12498.
(31) Wei, D.; Yang, J.; Jiang, M.-Q.; Dai, L.-H.; Wang, Y.-J.; Dyre, J. C.; Douglass, I.; Harrowell, P. Assessing the Utility of Structure in Amorphous Materials. *J. Chem. Phys.* **2019**, *150*, 114502.
(32) Rycroft, C. H. VORO++: A Three-Dimensional Voronoi Cell Library in C++. *Chaos* **2009**, *19*, 041111.
(33) Shannon, C. E. A Mathematical Theory of Communication. *Bell Syst. Tech. J.* **1948**, *27*, 379−423.
(34) Garside, K.; Henderson, R.; Makarenko, I.; Masoller, C. Topological Data Analysis of High Resolution Diabetic Retinopathy Images. *PLoS One* **2019**, *14*, No. e0217413.
(35) Anand, D. V.; Meng, Z.; Xia, K.; Mu, Y. Weighted Persistent Homology for Osmolyte Molecular Aggregation and Hydrogen-Bonding Network Analysis. *Sci. Rep.* **2020**, *10*, 9685.
(36) Obayashi, I. Volume-Optimal Cycle: Tightest Representative Cycle of a Generator in Persistent Homology. *SIAM J. App. Algebra Geometry* **2018**, *2*, 508−534.
(37) Obayashi, I. Https://Pypi.Org/Project/Homcloud/, June 1, 2021.
(38) Schneider, C. A.; Rasband, W. S.; Eliceiri, K. W. NIH Image to ImageJ: 25 Years of Image Analysis. *Nat. Methods* **2012**, *9*, 671−675.
(39) Atienza, N.; Gonzalez-Diaz, R.; Rucco, M. Persistent Entropy for Separating Topological Features from Noise in Vietoris-Rips Complexes. *J. Intell. Inf. Syst.* **2019**, *52*, 637−655.
(40) Vashishta, P.; Kalia, R.; Ebbsjo, I. Structural Correlations and Vibrational Spectra of Molten and Glassy GeSe2. *Solid State Ionics* **1989**, *32*−*33*, 872−881.
(41) Vashishta, P.; Kalia, R. K.; Antonio, G. A.; Ebbsjö, I. Atomic Correlations and Intermediate-Range Order in Molten and Amorphous GeSe2. *Phys. Rev. Lett.* **1989**, *62*, 1651−1654.
(42) Vashishta, P.; Kalia, R. K.; Ebbsjö, I. Structural Correlations and Phonon Density of States in GeSe2: A Molecular-Dynamics Study of Molten and Amorphous States. *Phys. Rev. B: Condens. Matter Mater. Phys.* **1989**, *39*, 6034−6047.
(43) Plimpton, S. Fast Parallel Algorithms for Short-Range Molecular Dynamics. *J. Comput. Phys.* **1995**, *117*, 1−19.
(44) Tilocca, A. Cooling Rate and Size Effects on the Medium-Range Structure of Multicomponent Oxide Glasses Simulated by Molecular Dynamics. *J. Chem. Phys.* **2013**, *139*, 114501.
(45) Gale, J. D. GULP: A Computer Program for the Symmetry-Adapted Simulation of Solids. *J. Chem. Soc., Faraday Trans.* **1997**, *93*, 629−637.
(46) Sørensen, S. S.; Biscio, C. A. N.; Bauchy, M.; Fajstrup, L.; Smedskjaer, M. M. Revealing Hidden Medium-Range Order in Amorphous Materials Using Topological Data Analysis. *Sci. Adv.* **2020**, *6*, No. eabc2320.

https://doi.org/10.1021/acsomega.2c01359
ACS Omega 2022, 7, 23255−23264